JOURNAL OF THERMOPHYSICS AND HEAT TRANSFER
Vol. 17, No. 2, April–June 2003

Transient Convective Effects on Diffusion Measurements in Liquids

John P. Kizito,* J. Iwan D. Alexander,†
Case Western Reserve University, Cleveland, Ohio 44106
and
R. Michael Banish‡
University of Alabama in Huntsville, Huntsville, Alabama 35899

The transient effects of convective disturbances on self-diffusivity measurements are evaluated using numerical simulations. "Codastefano-type" diffusivity measurements, where continuous real-time measurements of the concentration of the diffusing species are made at two discrete locations using a radioactive tracer, are considered. Convection arises due to buoyancy caused by the interaction of temperature gradients with either gravity (terrestrial experiments) or residual acceleration (microgravity experiments). For small deviations from ideal isothermal conditions, the system's response to residual microgravity disturbances is examined. The consequences of heating and cooling "temperature ramps" are also examined for both microgravity and terrestrial conditions. The frequency, amplitude, and orientation of the residual acceleration vector and the magnitude of heating or cooling rates all affect the fidelity of a given measurement. It is also shown that, for actual high-temperature experiments, it is important to assess the degree of isothermality that can be attained.

Introduction

BENCHMARK experiments to elucidate the temperature dependence of self-diffusion coefficients in liquid metals are planned for the International Space Station.[1] As part of the design of the experimental facilities and for experiment planning purposes, the effects of time-dependent environmental factors that can lead to undesirable disturbances of the experiments need to be assessed quantitatively. The desired outcome of the present experiments is to obtain diffusivity values within 1% of the actual diffusivity D. The potential contamination of diffusivity measurements due to convection caused by spacecraft residual acceleration, or g jitter, is of obvious concern. Temperature ramping (necessary in space experiments to examine the temperature dependence of the diffusivities efficiently) inevitably leads to transient temperature gradients that induce buoyancy flows. Such flows could result in significant contributions to the transport of the tracer and, thus, affect the measured value of the diffusivity. Even after the desired operating temperature has been obtained at the elevated operating temperatures necessary to study the temperature dependence of liquid metals, truly isothermal conditions may be impossible to achieve.

Neither self-diffusion in liquid elements or binary diffusion in molten alloys is sufficiently well characterized.[1] Indeed, based on experimental results, there is little agreement on the temperature T, dependence of diffusivity $D(T)$, and its correlation to the temperature-dependent structure of the liquid. Although various theories for $D(T)$ have been advanced, uncertainties in available experimental data[2–5] persist to the extent that unambiguous evaluation is not yet possible. Currently, the differences between $D(T)$ predicted by different theories are often less than the differences in $D(T)$ data sets measured in the same system. It is generally accepted that the variations in experimental data can be attributed to convective contamination. That is, for many systems, convection is unavoidable under terrestrial conditions.[6] However, it appears that the low-gravity environment of a low-Earth-orbit space laboratory will provide suitable conditions for self-diffusivity measurements in high-temperature liquid metals, provided that the levels of convection induced by residual microgravity acceleration do not significantly affect the transport conditions.

Several papers have demonstrated the reliability of numerical models for the analysis of the g sensitivity of directional solidification experiments. (See, for example, Refs. 7–11 and references therein.) The effect of steady acceleration on diffusivity measurements under terrestrial conditions was examined in a previous paper.[4] In such papers, the analyses were mostly based on two-dimensional numerical models of the actual experiments, although three-dimensional calculations, similar to those in Ref. 6, have also been carried out. The obvious advantage of a two-dimensional model is that it requires less computer time. Whereas two-dimensional calculations tend to overestimate the sensitivity to g jitter compared to three-dimensional calculations,[7] they nevertheless determine whether experimenters need be concerned about the impact of microgravity disturbances on their experiments.

Model Description

Self-Diffusion in Liquid Elements Measurement Technique

The self-diffusion in liquid elements (SDLE) experiment is currently being planned for the International Space Station. The experiment is a modification of a tracer technique based on a method originally developed by Codastefano et al.[12] A detailed description of the experiment is found in Refs. 1 and 13. Diffusivities are deduced in situ and in real time from concentration histories inferred from radioisotope emission time series obtained using a multiple detector arrangement. Two detectors are positioned at $L/6$ and $5L/6$ of the sample length, as depicted in Fig. 1. The precise sample length is dependent on the measurement temperature. At specified time intervals, the tracer activity is simultaneously monitored at the two locations. Hardware utilizing this approach to measure diffusion coefficients in molten indium has already been used under NASA sponsorship on the Mir space station.[3]

Received 23 June 2000; revision received 30 September 2002; accepted for publication 4 October 2002.

*Staff Scientist, National Center for Microgravity Research on Fluids and Combustion, NASA John H. Glenn Research Center at Lewis Field. Member AIAA.

†Professor, Department of Mechanical and Aerospace Engineering and Chief Scientist, National Center for Microgravity Research on Fluids and Combustion. Member AIAA.

‡Associate Director, Center for Microgravity and Materials Research; john.kizito@grc.nasa.gov. Member AIAA.

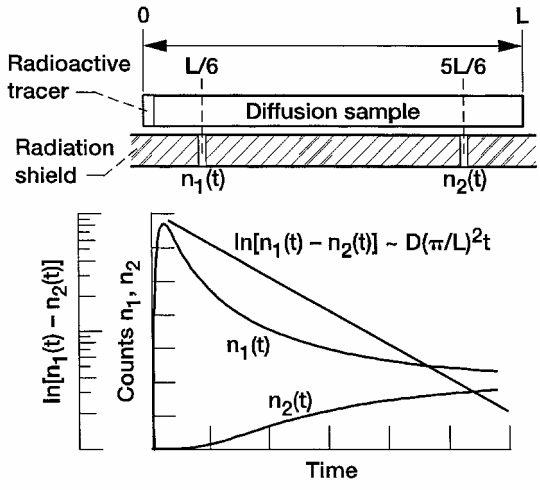

Fig. 1 Description of the "Codastefano-type"[12] tracer experiment (see Ref. 1).

Disturbances to purely diffusive transport conditions arise from a number of sources. In particular, buoyancy-driven flow arises from temperature gradients that occur during changes in operating temperature and due to heat losses that cause deviations from nonisothermality. When a nonuniform temperature field exists in an acceleration field, convective contamination of the diffusivity measurement can occur that augments or diminishes the diffusion coefficient values. The acceleration fields may be approximately uniform (terrestrial gravity or gravity-gradient type acceleration) or nonuniform due to vibration effects (g jitter).

Modeling Sensitivity to Residual Acceleration

We consider a closed rectangular region (two-dimensional) filled with liquid indium. The thermal boundary conditions imposed on the rigid bounding wall results in a temperature gradient such that, whenever the temperature gradient is normal to a body force vector, motion ensues. A simple, two-dimensional configuration is considered adequate to establish the order of magnitude sensitivities; a more detailed quantitative solution (if warranted) requires consideration of the full three-dimensional geometry.

Basic Equations

The basic equations that describe the system under investigation are rendered nondimensional using L, L^2/κ, and κ/L as scale factors for length, time, and velocity, respectively. Here, L is the length of the diffusion sample, and κ is thermal diffusivity. The aspect ratio (AR = width/length) is fixed at AR = 0.1 to comply with the aspect ratio used in actual experiments.[1]

Under the assumption that the Boussinesq approximation holds, the nondimensional governing equations are

$$\frac{\partial \boldsymbol{u}}{\partial t} + (\boldsymbol{u}\cdot\nabla)\boldsymbol{u} = -\nabla p + Pr\nabla\cdot[2\nu(\theta)\boldsymbol{D}] + (Ra\cdot Pr\cdot T)\boldsymbol{g} \quad (1)$$

$$\nabla\cdot\boldsymbol{u} = 0 \quad (2)$$

$$\frac{\partial\theta}{\partial t} + (\boldsymbol{u}\cdot\nabla)\theta = \nabla^2\theta \quad (3)$$

$$\frac{\partial c}{\partial t} + (\boldsymbol{u}\cdot\nabla)c = \frac{Pr}{Sc}\nabla\cdot[D(\theta)\nabla c] \quad (4)$$

where $\boldsymbol{u}$, p, θ, and c are the dimensionless velocity, pressure, temperature, and tracer concentration, respectively, and $\boldsymbol{D} = 1/2(\nabla\boldsymbol{u} + \nabla\boldsymbol{u}^T)$ is the rate of deformation tensor. The parameters $Pr = \nu/\kappa$, $Ra = \beta\Delta T g H^3/(\nu\kappa)$, and $Sc = \nu/D_0$ are the Prandtl, Rayleigh, and Schmidt numbers, respectively, where ν is the kinematic viscosity, β is the thermal expansion coefficient, and D_0 is the reference solute diffusivity. The nondimensional temperature is

$$\theta = \frac{[T(\boldsymbol{x},t) - T_m]}{(T_w - T_m)} \quad (5)$$

where T_m is the melting temperature of the liquid metal and T_w is the maximum temperature of the ampoule wall for given experiment. The vector $\boldsymbol{g}$ in Eq. (1) specifies the magnitude and orientation of the gravity vector or relative acceleration, which may be time dependent. For a reference frame fixed to the wall of the container, the motion of the rigid wall corresponding to a translational vibration appears as a body force.[10] For single-frequency oscillatory modulations of a steady acceleration, we use

$$\boldsymbol{g} = g^*[1 + b\Omega^2\cdot\sin(\Omega\cdot t)] \quad (6)$$

The factor $b\Omega^2$ is the product of a displacement amplitude and angular frequency. For situations where we examine the effects of temperature ramps, we account for changes in viscosity and diffusivity with temperatures. To account for changes in viscosity with temperature, the kinematic viscosity is taken to be

$$\nu(\theta) = \nu_0\cdot\exp(\chi\cdot\theta) \quad (7)$$

where $\nu_0 = 2.8\times10^{-3}$ cm^2/s and $\chi = -2.1$. These parameters were found to fit the thermophysical property data for indium reported in Ref. 6 and references therein. We account for temperature dependence of the tracer diffusivity simply by assuming that it has a quadratic dependence on temperature (consistent with one of the possible models being tested by the actual space-flight experiments). Whereas, for the systems under investigation, this might not be the correct dependence, it does increase the diffusivity magnitude. This means that, as far as sensitivity to convection is concerned, the increased magnitude of temperature gradients expected at higher temperatures is offset by the increase in effective diffusive transport velocity, thus allowing the system to tolerate larger convective velocities. The form of the temperature dependence was taken to be

$$D(\theta) = D_0(1 + \alpha\theta^2) \quad (8)$$

where $\alpha = 5.6$ and $D_0 = 1.48\cdot10^{-5}$ cm^2/s.

The following temperature boundary conditions were used. To model the "heatup" or to ramp down to a cooler temperature, we impose a uniform time-dependent temperature on all walls, enforce no-slip conditions for the velocity, and assume that the tracer does not penetrate the ampoule walls. That is,

$$\theta_w = \Lambda\cdot t, \qquad \vec{\boldsymbol{u}} = \boldsymbol{0}, \qquad \nabla C\cdot\vec{\boldsymbol{n}} = 0 \quad (9)$$

To model the initially thin strip of tracer at one end of the ampoule, we take the initial conditions at $z \le 0.1$ to be

$$c(\boldsymbol{x},0) = 1, \qquad \boldsymbol{u}(\boldsymbol{x},0) = \boldsymbol{0}, \qquad \theta(\boldsymbol{x},0) = 0 \quad (10)$$

For $z > 0.1$,

$$c(\boldsymbol{x},0) = 0, \qquad \boldsymbol{u}(\boldsymbol{x},0) = \boldsymbol{0}, \qquad \theta(\boldsymbol{x},0) = 0 \quad (11)$$

The subscript i refers to the initial condition, and Λ represents the heating rate. The preceding boundary conditions are ideal because temperature deviations of up to ±5°C can occur in actual experiments.[14] To simulate these deviations from isothermality, a uniform temperature gradient is modeled as shown in Fig. 2, which shows a deviation ε from the desired uniform temperature on one ampoule wall of 0.1–0.5%. Note that $\varepsilon = 10^{-3}$ represents 1°C in 1000°C. The imposed temperature is then given by the following. For the right wall,

$$\theta_w = \Lambda\cdot t\cdot(1 + \varepsilon) \quad (12a)$$

For the left wall,

$$\theta_w = \Lambda\cdot t \quad (12b)$$

For the top and bottom walls,

$$\theta_w = \Lambda\cdot t\cdot(1 + \varepsilon x) \quad (12c)$$

Because over the temperature ranges being considered, thermophysical properties vary with temperature, we account for the variation in melt viscosity and tracer diffusivity with temperature by using

Table 1 Values of thermophysical properties according to simulations

T, K	Pr	Sc	$10^4\ \nu$	$10^5\ D$
1429	0.0031	3.49	3.43	9.80
1073	0.0066	14.69	7.24	4.93
873	0.0100	35.26	11.00	3.12
673	0.0153	84.85	16.80	1.98
429	0.0255	189.1	28.00	1.48

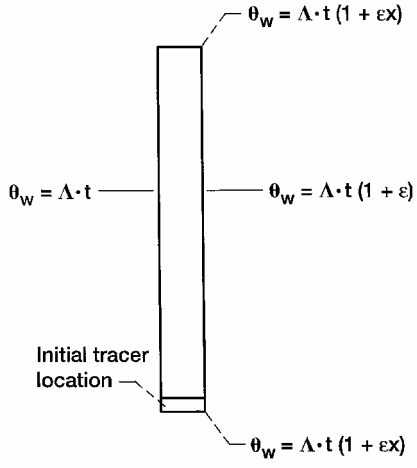

Fig. 2 Thermal boundary conditions and initial tracer location.

the viscosity corresponding to the desired (uniform) operating temperature. The small variations in viscosity and tracer diffusivity due to small deviations from this reference temperature are neglected. (Specific values of the viscosity and diffusivity used at different temperatures are presented in Table 1.)

Modeling *g* Jitter and Vibration

Motivated by the frequencies expected aboard the International Space Station, only low-frequency g jitter in the range 0.001–10 Hz was examined. Impulse accelerations taken from space acceleration measurement system (SAMS) acceleration data[12,15–17] are used to assess the effects of short-lived disturbances. Impulses that result in acceleration normal to the temperature gradients were considered because they result in the largest convective velocities.

Shear-Cell Technique

An alternative to the Codastefano et al.[12] technique is the shear-cell method. This method is used for diffusivity measurements in a binary melt.[18] The shear-cell technique was devised to minimize errors associated with the process of solidification during diffusion measurement techniques that require rapid quenching of the sample to preserve the concentration profile. The shear-cell ampoule is composed of vertically stacked cylindrical sections that can be rotated (sheared) in a plane perpendicular to the cylinder axis, such that any transfer of material between the volumes enclosed by each section is prevented. The idea behind the shear-cell technique is initially to bring two liquid columns of different composition into contact, whereupon interdiffusion occurs. After a specified elapsed time, the sample is sheared into several sections. These are subsequently quenched. The diffusivity is then determined from the composition profile determined from compositional analysis of the quenched sections. (See Arnold and Matthiesen[18] for more details.) After terminating the experiment at a suitable time t^*, shearing the sample into multiple sections, and quenching, D' is then obtained graphically from the slope of $\ell n[c(z, t^*)]$ vs z^2 (the axial coordinate parallel to the diffusion direction). The $c(z, t^*)$ profile is reconstructed from concentration values that represent the average concentration determined from the chemical analysis of each section. Thus, the solution is dependent on the spatial accuracy of the $c(z, t^*)$ data. To address whether the initial and the final shearing events can adversely affect the final diffusivity measurements, we simulate the flows induced by the shearing and the effects on the concentration profile.

Numerical Method

The equations and their boundary conditions are solved numerically using third-order upwinding for convection and a simultaneous overrelaxation-alternating direction implicit (SOR-ADI) technique on a constant, evenly spaced grid. The width-to-length ratio AR for the cells under investigation was 0.1. Grid-dependence tests showed that 50×400 (width $\times$ length) grid points is adequate for a two-dimensional simulation for the conditions investigated.

Results and Discussion

First, we discuss the results for the SDLE model under pure diffusion and for conditions where transient buoyant convection is present. Then, we discuss the initial and final shearing events in a shear-cell experiment.

SDLE: Pure Diffusion Measurements

The ideal environment for diffusivity measurements is one where all buoyancy forces are zero. (For self-diffusion, this corresponds to purely isothermal conditions.) For purely diffusive conditions, the results of the simulation are presented in Table 2 and in Figs. 3 and 4. Figure 3 shows the heating model that is applied in the present analysis with a heating rate of 15 K/min to obtain a temperature range of 1000 K above the melting point. A rate of 5 K/min was also used, which is the lower limit for data collection. For a given temperature, the slope of $\ell n(c_1 - c_2)$ in Fig. 4 (where c_1 and c_2 are the normalized average concentrations at $L/6$ and $5L/6$, respectively) is proportional to the diffusivity, provided that sufficient time has

Table 2 Results for pure diffusion (using concentration data from *L*/6 and 5*L*/6)

T, K	Input $10^5\ D$, cm^2/s	Results $10^5\ D$, cm^2/s	% Error
1429	9.80	9.71	0.92
1173	6.0854	6.0859	−0.0082
1073	4.930604	4.930632	−0.0006
973	3.942188	3.942174	0.0004
873	3.120172	3.120157	0.0005
773	2.464556	2.464542	0.0006
673	1.975340	1.975331	0.0005
573	1.652524	1.652513	0.0007

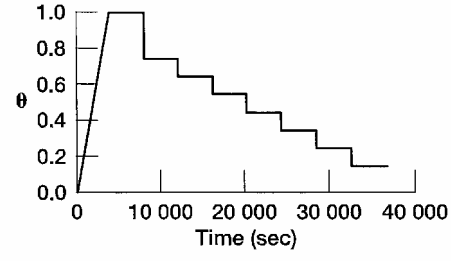

Fig. 3 Dimensionless operating temperature θ as a function of time; the dimensionless heating rate was corresponding to an actual heating rate of 15 K/min.

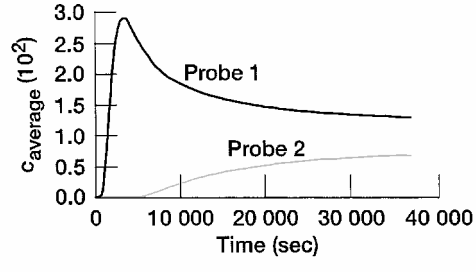

Fig. 4 Average concentration monitored at *L*/6 and 5*L*/6 corresponding to the temperature ramp profile shown in Fig. 3.

elapsed since the start of the experiment or since the end of a temperature ramp. For accurate calculation of the diffusivity from the measured data, it is best to start using data taken after both detectors register significant concentrations and after the reading at the first detector has started to decay exponentially. Following startup or after a change in temperature, this takes between 4–5000 s for the diffusivities listed in Table 2.

Terrestrial Conditions (1 *g*)

Figure 5 shows the effect of convection caused by the decrease in temperature on the concentration time history at $L/6$, together with the corresponding temperature ramp profile at the wall. (Note the sudden drop in concentration coincident with the abrupt temperature change during the ramp-down phase.) Changing the wall temperature from 1429 to 1173 K causes the concentration monitored at the $L/6$ probe to suddenly decrease and that at the $5L/6$ probe to suddenly increase due to the abrupt increase in transport rate.

The value of D' at 1429 K in normal gravity is about 4% smaller than the input diffusivity, D. This can be explained by the flow pattern during the heating phase. Figure 6 shows that, in 1 *g*, before isothermal conditions are attained, the initial heating up to the highest operating temperature causes a significant deformation of concentration isolines due to a strong upward flow along the wall and a strong downflow in the center. The effect of gravity in this configuration is to produce a weak convective flow that actually hinders axial diffusion.

During heating, the fluid rises at the hotter walls and sinks in the colder core region. At the end of the heating phase, when the

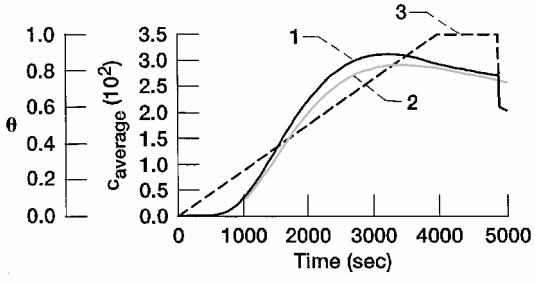

Fig. 5 Curves 1 and 2 correspond to concentration time histories measured at $L/6$ under 1 *g* and 0 *g*, respectively; curve 3 shows the corresponding temperature ramp.

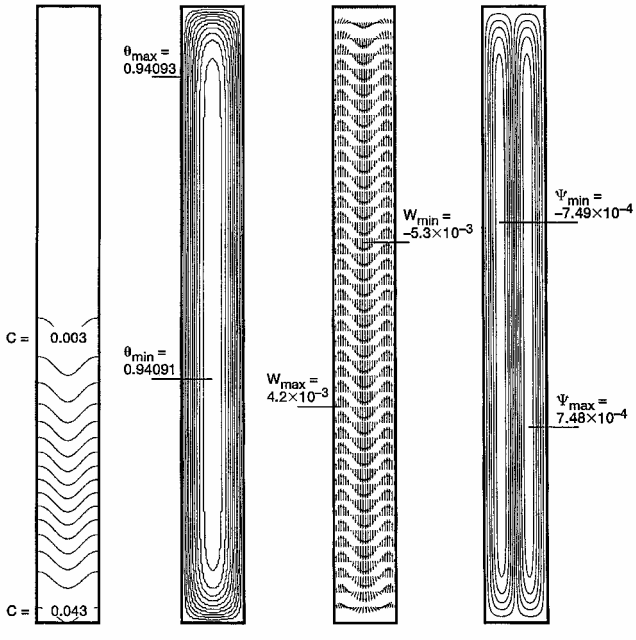

Fig. 6 Concentration, temperature, velocity, and stream-function contours at 3763 s during ramping to the new operating temperature.

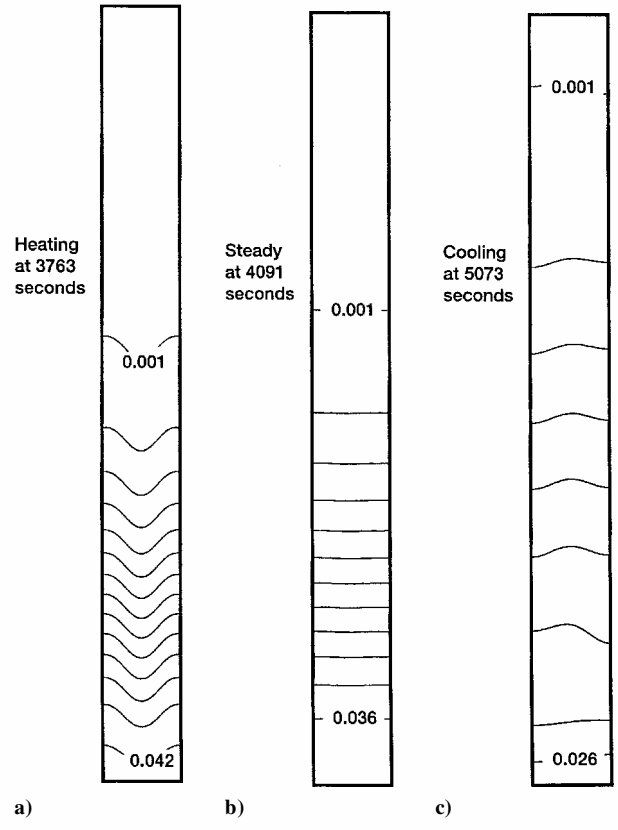

Fig. 7 Effect of nonuniform temperature on concentration during a) heating phase at 3763 s, b) steady isothermal phase, and c) cooling phase at 5073 s.

wall temperature is held at a constant value, the concentration isolines become almost horizontal. This is because buoyant convection is nonexistent under the ideal isothermal conditions illustrated in Fig. 7b. During cooling, the concentration isolines are deflected down at the walls and up in the core region because the core is hotter than the walls. It is clear that, for self-diffusivity measurements, the degree to which the system can be made isothermal is the most important factor in minimizing the convection contamination. This point is further illustrated by the results of a set of simulations, for which a temperature nonuniformity corresponding to 0.1% of every 1000 K above the melting point was deliberately introduced across the sample cell. Figure 8 shows that this eventually results in complete mixing of the tracer concentration. At 286 K above the melting point, convection resulted in a highly distorted concentration profile, and a meaningful diffusivity measurement could not be obtained.

The conclusion that can be drawn from these simulations is that, unless other means of suppression of convection are available, for example, using magnetic fields, diffusivity experiments in liquid metals in 1 *g* require ideal isothermal conditions if D is to be measured without significant convective contamination. Such conditions may be impossible to obtain at high operating temperatures.

In an actual experiment, the collimator windows (see Fig. 1) are one source of temperature nonuniformity on the ampoule wall. This is because the heaters view the ampoule wall directly, and in the vicinity of the collimator windows, radiation can lead to temperatures that are approximately 0.5% higher than the desired temperature. Figures 9 and 10 show the stream function, tracer concentration, and velocity vectors caused by convection, which is due to direct heat radiation at the collimator window. Comparing Figs. 9 and 10, one can conclude that there are additional contributions to buoyant convection that arise from local thermal asymmetry due to imperfect heating conditions. These contributions further distort the concentration field. All of this can adversely affect the fidelity of diffusivity measurements if the temperature nonuniformities become too large.

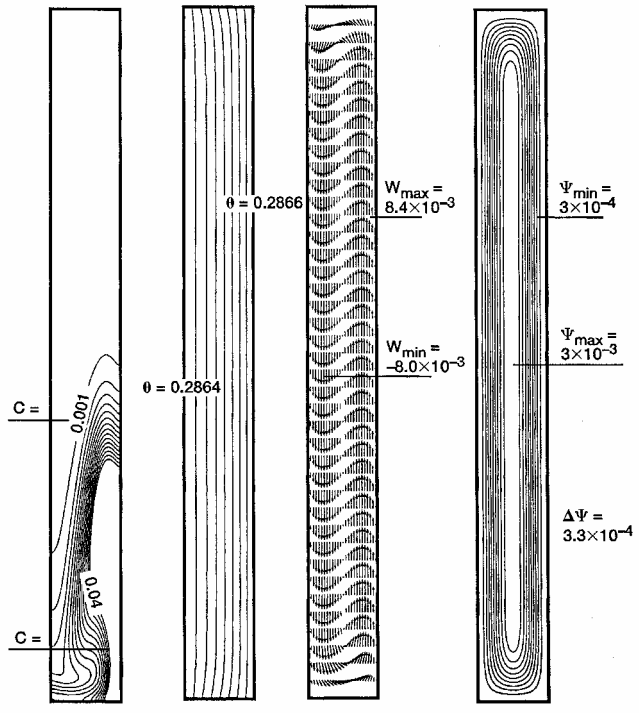

Fig. 8 Concentration profile as it progresses toward washout in 1 g with 0.1% linear temperature nonuniformity: concentration, temperature, velocity vectors, and stream-function contours at 1145 s.

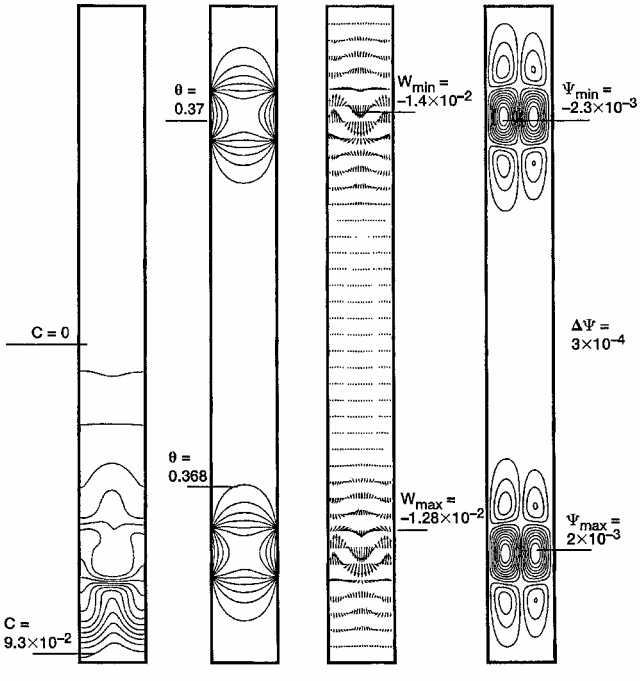

Fig. 9 Effect of collimator window on the concentration profile: concentration, temperature, stream-function contours, and velocity vectors at 1472 s.

Vibrational and g Jitter Response

To investigate the sensitivity of the self-diffusion experiments to g jitter and vibration characteristics of the low-g environment of a low-Earth-orbit spacecraft, we investigated both impulse-type and sinusoidal disturbances. Thruster firing events (impulses) were modeled as square waves. An extreme example of such an event is a main engine firing. This was simulated, and the effects are shown in Fig. 11. A single orbiter main system (OMS) thrust (magnitude $\sim 5 \times 10^{-2}$ g for 30 s) during the measurement of D is enough to contaminate the measurement at 1000 K above the melting point.

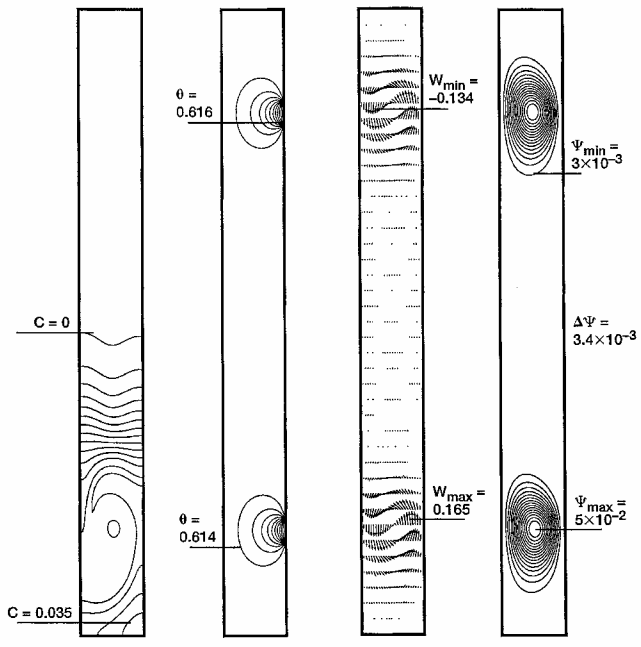

Fig. 10 Effect of nonsymmetrical collimator window on the concentration: concentration, temperature, stream-function contours, and velocity vectors at 2456 s.

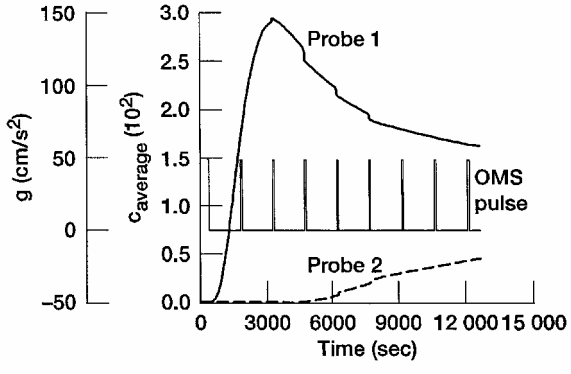

Fig. 11 Average concentration as a function of time and the square wave gravity pulse.

At 1429 K, three impulses yield $D' = 12.6 \times 10^{-5}$ cm^2/s compared to the input value $D = 9.8 \times 10^{-5}$ cm^2/s, that is, an error of 28%. At 1173 K, the effect of an OMS burn was reduced considerably, and the data yielded D' within 5% of the input D. These simulations were carried out with a heating nonuniformity of 0.1% of the type described earlier. When the pulse magnitude was reduced to 0.01 g_0, the error in D measurements was less that 1%. Further reduction of the pulse magnitude to 0.005 g resulted in $D' = D$. Primary reaction control system (PRCS) thrusts typically have magnitudes between 10^{-3}–10^{-2} g_0 and last for short times, typically, less than a second. These were found to have no significant influence on D'.

Vibrations and other periodic accelerations are also a concern, particularly at low frequencies. The low frequencies (0.001–1 Hz) examined here were found to affect D' only slightly, although the convective effects increased with increasing amplitude.

Simulations of Shear-Cell Experiments

When shear cells are used, an additional convection contamination is introduced that depends on the shear rate and the number of cells in the shear-cell arrangement. First, we considered the initial shearing event that brings a thin layer of the tracer into contact with the rest of the melt. We simulated the initial shearing by imposing a velocity of 1 cm/s on the separator between the two samples. The no-slip condition ensures that the separator drives the underlying fluid, but, as it is withdrawn, fluid no longer in contact with the

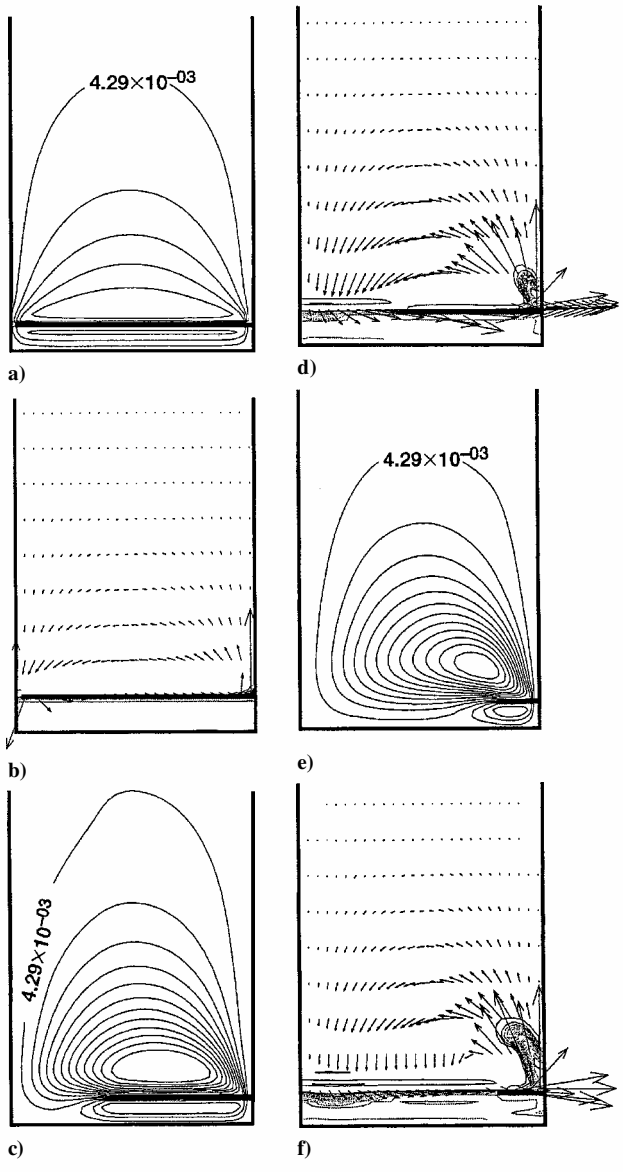

Fig. 12 Initial shear process: the tracer is initially separated from the melt by a region of thickness h; the melt and tracer are brought into contact by the withdrawal of the separator from the right at a fixed speed: a), c), and e) stream-function contours at times 0.02 s, 0.2 s, and 0.4 s and b), d), and f) velocity vectors with concentration isolines superimposed at times 0.02 s, 0.2 s, and 0.4 s.

separator is no longer dragged at the separator velocity. Figure 12 depicts the deformation of the initial profile due to shear. (The separator is withdrawn from the right in each of Figs. 12a–12f.) The process occurs in less than 0.5 s and the kinetic energy imparted is dissipated within 3 s. Figure 12 also shows that the penetration of the convection caused by shearing is larger than the cell width. However, the length scale over which significant mixing of the tracer occurs is much smaller, but, nevertheless, significant. Whereas the kinetic energy decays quickly, its effect on the concentration profile lasts much longer (Fig. 13). It takes about 2500 s for the concentration isolines to recover from the initial shearing.

The evolution of concentration isolines is shown in Fig. 13 at 0.4, 12.7, 119, 605, 1700, and 2549 s. The corresponding maximum relative concentrations are 1.125, 1.02, 0.66, 0.26, 0.127, and 0.08, respectively. As the results show, one cannot use the kinetic energy decay time to draw conclusions as to the temporal effects of a disturbance. This may lead to an erroneous conclusion as to whether the initial shear affects the final measurement. Indeed, it is better to wait for a period on the order of the characteristic diffusion time before ending an actual experiment. This will ensure that the effects of the initial shear are no longer remembered. (This is illustrated in

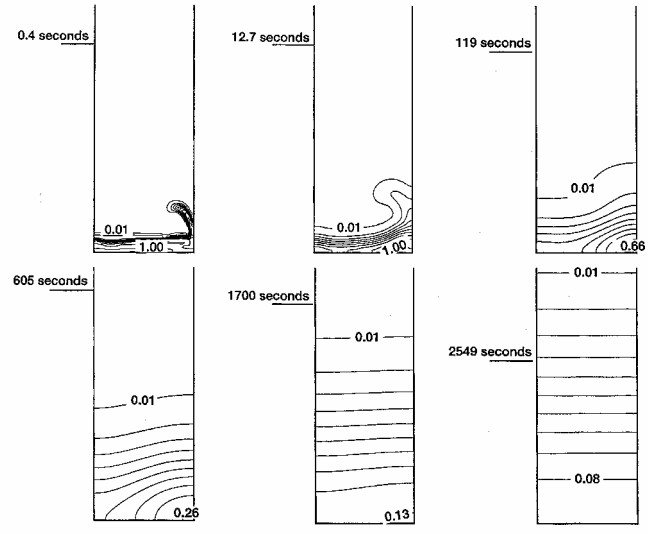

Fig. 13 Evolution of the concentration profile during the heating process after the initial shearing action.

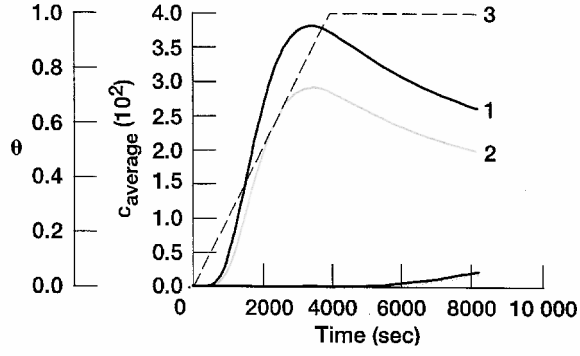

Fig. 14 Curves 1 and 2 correspond to concentration time histories measured at $L/6$ under shear cell and pure diffusion, respectively, and curve 3 shows the corresponding temperature ramp.

Fig. 13f, where it is seen that the concentration isolines are parallel to the width of the ampoule.)

The shearing action has also been evaluated for its effect on the measurement of $D(T)$, as shown in Fig. 14. Figure 14 shows the average concentration monitored at $L/6$ and $5L/6$. The corresponding temperature profile at the wall is also included. Clearly, shearing has an effect on the evolution of the concentration profile. However, the effect is essentially uniform throughout the sample, as evidenced by the slope of the concentration vs time at times greater than 4500 s. This suggests that the initial shearing, combined with the real-time Codastefano et al.[12] technique would not affect the measurement if D' is calculated from data collected after the second detector starts to receive an appreciable signal.

At the end of a shear-cell experiment, the ampoule is sheared into several segments and quenched. The concentration of each segment is then averaged to construct a profile from which the diffusion coefficient is calculated. The results of a simulation of the final shearing are presented hereafter.

Figure 15 compares a final concentration profile and flowfields before and after the final shearing of the sample into 10 segments after 32,728 s have elapsed. The concentration fields are shown with the corresponding stream-function contours. The convective velocities are much smaller than the diffusion velocity scale. The background residual acceleration is steady, with magnitude $10^{-6}\, g_0$, and the shearing lasts for less than 0.4 s.

Figure 15b shows the concentration fields and stream-function contours immediately after shearing. Even before quenching, the concentration distribution is affected. Figure 15 shows that concentration vs the square of the diffusion coordinate are no longer straight lines and that they also vary spatially. However, if the concentration

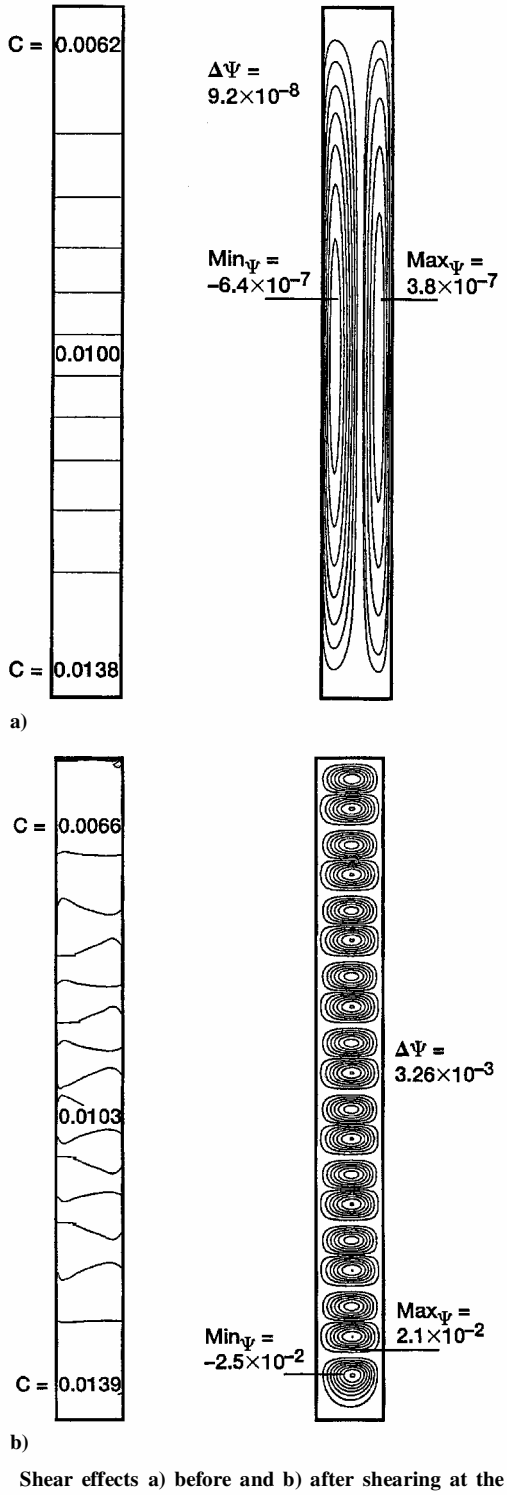

Fig. 15 Shear effects a) before and b) after shearing at the end of the experiment on the concentration profile and the stream-function contours, 32,728 s after the start.

in the sheared blocks is averaged and compared with the initial profile at a location corresponding to midpoints of the cells, the concentration values lie on the diffusion curve if the gradients are not too steep. Thus, it appears that shearing may not significantly affect the measurement.

Conclusions

The effects of deviations from isothermal conditions in self-diffusion experiments conducted under terrestrial and low-gravity conditions have been examined. It is shown that, under terrestrial conditions, during the initial heating phases, and when the temperature is ramped down to a new operating temperature, buoyant convection will contaminate the diffusivity measurement.

We found that the most important condition is the degree of isothermality, regardless of the gravitational environment, and that these should be minimized. However, in low-gravity conditions characteristic of a low-Earth-orbit spacecraft, we found that the reduction in g level was sufficient to guarantee that the measured diffusivity was uncontaminated by convection, except in the extreme case of long-duration 5×10^{-2} g impulses characteristic of main engine burns.

Acknowledgments

The authors gratefully acknowledge the support of the NASA through grants NCC8-99 and NAG8-1476.

References

[1]Jalbert, L. B., Banish, R. M., and Rosenberger, F., "Real-Time Diffusivity Measurements in Liquids at Several Temperatures with One Sample," *Physical Review E*, Vol. 57, No. 2, 1998, pp. 1727–1736.

[2]Careri, G., Paoletti, A., and Vincentini, M., "Further Experiments on Liquid Indium and Tin Self-Diffusion," *Nuovo Cimento*, Vol. 10, No. 6, 1958, pp. 1088–1099.

[3]Lodding, V. A., "Selbstdiffusion in Geschmolzenem Indiummetall," *Zeitschrift für Naturforsching*, Vol. 11a, No. 3, 1956, pp. 200–203.

[4]Foster, J. P., and Reynik, R. J., "Self-Diffusion in Liquid Tin and Indium over Extensive Temperature Ranges," *Metallurgical Transactions*, Vol. 4, No. 1, 1973, pp. 207–217.

[5]Oglobya, V. I., Lozovoi, V. I., and Chumakov, A. G., "Atomic and Group Diffusion Coefficients in Liquid Metals," *Physics of Metals and Metallography*, Vol. 9, 1990, pp. 455–460.

[6]Alexander, J. I. D., Ramus, J. F., and Rosenberger, F., "Numerical Simulations of the Convective Contamination of Diffusivity Measurements in Liquids," *Microgravity Science and Technology*, Vol. 9, No. 3, 1996, pp. 158–162.

[7]Alexander, J. I. D., Ouazzani, J., and Rosenberger, F., "Analysis of the Low-Gravity Tolerance of Bridgman–Stockbarger Crystal Growth I," *Journal of Crystal Growth*, Vol. 97, No. 2, 1989, pp. 285–302.

[8]Garandet, J. P., Corre, S., Gavoille, S., Favier, J. J., and Alexander, J. I. D., "On the Effect of Gravity Perturbations on Composition Profiles During Bridgman Crystal Growth in Space," *Journal of Crystal Growth*, Vol. 165, No. 4, 1996, pp. 471–481.

[9]Nelson, E., and Kassemi, M., "The Effects of Residual Acceleration on Concentration Fields in Directional Solidification," AIAA Paper 97-1002, 1997.

[10]Alexander, J. I. D., Amiroudine, S., Ouazzani, J., and Rosenberger, F., "Analysis of the Low-Gravity Tolerance of Bridgman–Stockbarger Crystal Growth II," *Journal of Crystal Growth*, Vol. 113, Nos. 1–2, 1991, pp. 21–38.

[11]Favier, J. J., Rouzaud, A., and Comera, J., "Influence of Various Hydrodynamic Regimes in a Melt on a Solidification Interface," *Revue de Physique Appliquee*, Vol. 22, No. 8, 1987, pp. 713–718.

[12]Codastefano, P., Di Russo, A., and Zanza, A., "New Apparatus for Accurate Diffusion Measurements in Fluids," *Review of Scientific Instruments*, Vol. 48, No. 12, 1977, pp. 1650–1653.

[13]Alexander, J. I. D., and Banish, R. M., "Modeling g-Sensitivity of Low-Gravity Experiments," *Microgravity Science and Technology*, Vol. 11, No. 3, 1998, pp. 90–95.

[14]Alexander, J. I. D., "Crystal Growth Experiments and Residual Accelerations," *Materials and Fluids Under Low Gravity*," edited by L. Ratke, H. Walter, and B. Feuerbacher, Springer, Berlin, 1995, pp. 95–100.

[15]Alexander, J. I. D., Favier, J. J., Garandet, J.-P., and Lizee, A., "g-Jitter Effects on Segregation During Directional Solidification of Tin–Bismuth in the MEPHISTO Furnace Facility," *Journal of Crystal Growth*, Vol. 178, No. 4, 1997, pp. 657–661.

[16]Jalbert, L. B., "Multi-Temperature in situ Radiotracer Self-Diffusion Measurements in Liquid Elements," Ph.D. Dissertation, Dept. of Physics, Univ. of Alabama in Huntsville, Huntsville, AL, July 1997.

[17]Favier, J. J., Garandet, J. P., Rouzaud, A., and Camel, D., "Mass Transport Phenomena During Solidification in Microgravity: Preliminary Results of the First MEPHISTO Flight Experiment," *Journal of Crystal Growth*, Vol. 140, Nos. 1–2, 1994, pp. 237–243.

[18]Arnold, W. A., and Matthiesen, D., "Numerical Simulation of the Effect of Shearing on the Concentration Profile in a Shear Cell," *Journal of the Electrochemical Society*, Vol. 142, No. 2, 1995, pp. 433–439.